

EVLA MEMO # 73

RESULTS OF WATER VAPOUR RADIOMETRY TESTS AT THE VLA

C. J. Chandler, W. F. Brisken, B. J. Butler, R. H. Hayward,
and B. E. Willoughby

NRAO, Socorro

August 09, 2004

SUMMARY

We report on the results of one year of tests of a three-channel water vapour radiometer (WVR) on two VLA antennas. The output from one of the circularly-polarized feeds of a standard VLA 22-GHz receiver is split on exiting the dewar; one signal path leads to a temperature-stabilized plate on which the WVR detection system is mounted, the other leads to the normal astronomical system electronics. We measure the correlation between fluctuations in astronomical phase (assumed to be dominated by the troposphere), ϕ , and the WVR difference output from the two antennas, on various timescales. We find that in all cases applying a correction derived from the WVR improves the rms phase, for observing frequencies ranging from 8 GHz to 43 GHz. The improvement is most dramatic when the sky is clear and the tropospheric phase fluctuations are large. When there are clouds present the WVR output is contaminated by the fluctuations in system temperature caused by liquid water, and the correlation between ϕ and the WVR output is not as good. However, even in this case the RMS phase is still improved by applying a correction derived from the correlation.

1. BACKGROUND TO WATER VAPOUR RADIOMETRY

The dominant source of phase fluctuations for the EVLA at high frequencies ($\nu \gtrsim 5$ GHz) will be fluctuations in the water vapour content of the troposphere. One millimetre of precipitable water vapour (PWV) causes ~ 6.3 mm excess vacuum equivalent electrical path, and the combination of temporal and spatial fluctuations in the water vapour can decorrelate the signal from an astronomical source to the extent that the source may not be detected or imaged unless it is strong enough for self-calibration techniques to work on timescales shorter than that of the fluctuations. In order to be able to image weak sources under marginal observing conditions a means of correcting for the phase fluctuations introduced by the troposphere must be developed. One method currently being explored at many of the millimeter-wave observatories around the world uses the fact that the atmospheric water vapour is also a source of both continuum and line emission. Fluctuations in the water vapour produce concomitant fluctuations in the sky emission, and measurements of these fluctuations via radiometry can then be used to derive corrections for the astronomical phase.

A complication is that liquid water is also a strong source of continuum emission ($T_B \propto \nu^2$), but does not contribute much to the electrical path. In the presence of liquid water the fluctuations in the sky emission may therefore not correlate well with the phase fluctuations, and is a problem especially for continuum radiometry. Under these circumstances one does better by observing one of the water vapour emission lines (e.g., 22 or 183 GHz), preferably with multiple frequency channels, so that the emission due to the water vapour can be disentangled from the liquid water. Ideally one of these channels should be well away from the water vapour emission line, so that the ν^2 continuum can be more easily distinguished from the vapour.

At the VLA site the 183 GHz water vapour line is too saturated to be used for measuring fluctuations in the water vapour. Instead we use the 22 GHz line, measured using a simple three-channel system. The channels are placed at the centre and on either side of the line, and to first order the water vapour emission can be isolated by subtracting a linear continuum, if the three channels are relatively closely spaced in frequency. For the example shown in Figure 1, the resulting “observable,” ΔT , is then

$$\Delta T = w_1 T_1 + w_2 T_2 + w_3 T_3$$

where the weights, w , are typically $w_1 = -0.5$, $w_2 = 1.0$, and $w_3 = -0.5$, and T_1 , T_2 , and T_3 are the brightness temperatures of the sky in the three channels.

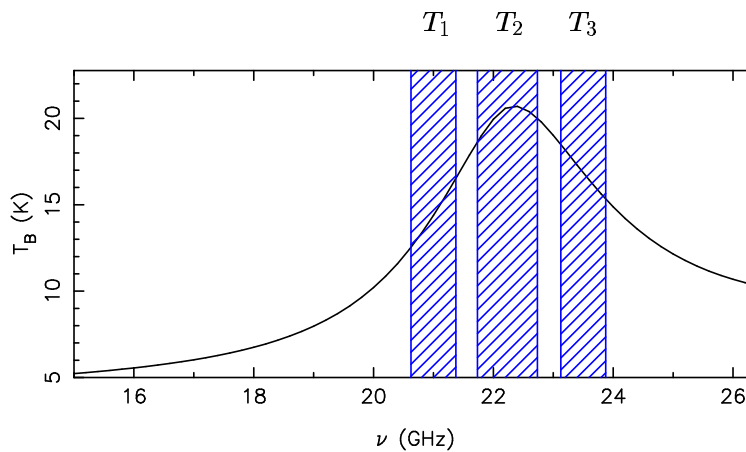


Figure 1: 22 GHz water vapour line with the location of the three channels used in the VLA water vapour radiometer marked (cf. Butler 1999).

2. DESIGN AND TESTING OF A WATER VAPOUR RADIOMETER FOR THE VLA

2.1. Stability Requirements

The amplitude of ΔT will be largest when the edge channels (channels 1 and 3 in Figure 1) are as far away from the centre channel as possible. For the VLA the location of the edge channels is unfortunately limited by power leaking in from the K-band local oscillator on the low frequency side, and the first harmonic of the X-band local oscillator on the high frequency side. The result is that the edge channels are actually very close to the centre of the water vapour line, as shown in Figure 1.

Butler (1999) describes in detail the stability requirements for a water vapour radiometer (WVR) with channel locations given in Figure 1. To summarize, the WVR must be able to correct for tropospheric phase fluctuations at the level of the intrinsic phase stability of the VLA electronics, which is typically

$$\Delta\phi_e \sim \frac{\nu_{\text{GHz}}}{4}$$

where ϕ_e is in degrees, and ν_{GHz} is the frequency in GHz. As an aside, this electronics noise is almost entirely due to the switching of the last delay bit for each antenna. This electronic noise floor is equivalent to $\sim 220 \mu\text{m}$ of electrical path delay ($\lambda/30$ for a wavelength of 7 mm), or $\sim 35 \mu\text{m}$ of PVW. By considering possible model atmospheres, Butler predicts that for the channel locations given in Figure 1, 35 μm of PVW will result in $\Delta T \sim 25 \text{ mK}$. For $\Delta T_{\text{rms}} \sim 25 \text{ mK}$ the stability of an individual channel needs to be $\sim 20 \text{ mK}$, which for typical system temperatures of 50–100 K implies a gain stability $\Delta g/g \sim 2\text{--}4 \times 10^{-4}$.

2.2. Design

We use the existing VLA K-band receivers for the WVR. Figure 2 shows a block diagram of the system: the output from the left circularly polarized feed is split on exiting the dewar, with one signal path leading to the normal astronomical detection system, and the other leading to the WVR detection system mounted on a temperature-stabilized plate. The main contributions to the overall gain stability of this system arise from receiver stability, the stability of the calibration signal from the noise diode, thermal noise, and the resolution of the digitizer (a voltage to frequency converter).

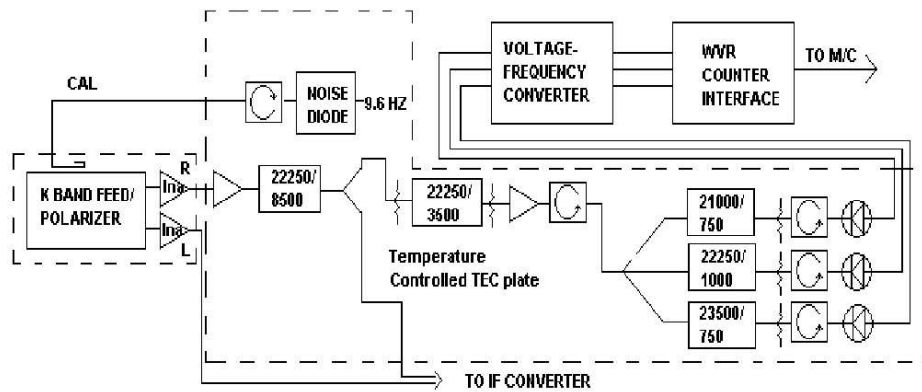


Figure 2: Block diagram of the VLA WVR system. The three channels are centred at the frequencies shown in Figure 1.

Table 1 gives the specifications of the various components of the system shown in Figure 2.

Table 1: Components of the VLA WVR.

Component	Manufacturer	Part no.	Specifications
First amplifier	Miteq	JS4-18002650-25-8P	35 dB gain, NF 2.0 dB
First filter	K & L	13FV10-22250/U8500-0/0	$\nu_0=22.25$ GHz, 8500 MHz bw (1.5 dB) min.
Splitter 2-way	Krytar	6020265	2–26.5 GHz
2nd filter	K & L	7FV05-22250/T3500-K/K	$\nu_0=22.25$ GHz, 3500 MHz bw (1.5 dB) min.
2nd amplifier	Miteq	JS4-18002650-25-8P	35 dB gain, NF 2.0 dB
Splitter 3-way	Narda	4B68-3	2–40 GHz
Filter channel 1	K & L	5FV10-21000/X1000-K/K	$\nu_0=21.00$ GHz, 1000 MHz bw (6 dB) max., 750 MHz (1.5 dB) min.
Filter channel 2	K & L	5FV10-22250/X1400-K/K	$\nu_0=22.25$ GHz, 1400 MHz bw (6 dB) max., 1000 MHz (1.5 dB) min.
Filter channel 3	K & L	5FV10-23500/X1000-K/K	$\nu_0=23.50$ GHz, 1000 MHz bw (6 dB) max., 750 MHz (1.5 dB) min.
Tunnel diode detectors	Advanced Control Components	ACTP-1799NC38 (matched set of 3)	Temp. coeff. and voltage sensitivities matched within 2% and 5% respectively
Isolators	Mica	T-318K01	18–26.5 GHz, 18 dB isolation min.
Digitizer (V–f)	Analog Devices	AD650	0–1 MHz

2.3. WVR Output

The square-law diode detectors provide measurements of the output voltage from each channel, both with and without the signal from the calibration noise diode. The noise diode is switched in and out of the signal path with 50% duty cycle with a period of 104 ms. The outputs are averaged over 8 cycles (0.83 seconds) to provide two voltage values: one with the noise diode off (V_{off}), and one with the noise diode on (V_{on}). Using measurements of the noise temperature of the calibration source, T_{cal} , the output from a single channel of the WVR is then

$$T = \left(\frac{T_{\text{cal}}}{\langle V_{\text{on}} - V_{\text{off}} \rangle} \right) V_{\text{off}}$$

where V_{off} includes contributions from the sky (V_{sky}), receiver noise, and spillover, and $\langle V_{\text{on}} - V_{\text{off}} \rangle$ is an average of $V_{\text{on}} - V_{\text{off}}$ over some timescale. If we assume that the receiver noise and spillover are only slowly varying, then the single channel output can be approximated as

$$T \approx \left(\frac{T_{\text{cal}}}{\langle V_{\text{on}} - V_{\text{off}} \rangle} \right) V_{\text{sky}} + \text{constant}$$

and the measurement of the observable, ΔT , is then

$$\begin{aligned} \Delta T = & w_1 \left(\frac{T_{\text{cal}}}{\langle V_{\text{on}} - V_{\text{off}} \rangle} \right)_1 (V_{\text{sky}})_1 + w_2 \left(\frac{T_{\text{cal}}}{\langle V_{\text{on}} - V_{\text{off}} \rangle} \right)_2 (V_{\text{sky}})_2 + \\ & w_3 \left(\frac{T_{\text{cal}}}{\langle V_{\text{on}} - V_{\text{off}} \rangle} \right)_3 (V_{\text{sky}})_3 + \text{constant}. \end{aligned}$$

ΔT is an antenna-based quantity.

2.4. Tests

WVRs of the design shown in Figure 2 have been installed on two VLA antennas, enabling field tests on a single baseline. For a baseline between antenna i and antenna j the measurement of the astronomical phase is a differential measurement, $\phi = \phi_i - \phi_j$; the relevant output of the WVR system on these two antennas to be compared with the phase measured on an astronomical source is therefore $\Delta T_{\text{diff}} = \Delta T_i - \Delta T_j$. Initial values of T_{cal} for each channel are estimated from laboratory measurements obtained using ambient and cold loads every 100 MHz across the bandpass of the K-band receiver, and averaged for the filter bandpasses given in Table 1 assuming a flat bandpass response. Final values of T_{cal} are measured once the receiver has been installed in the antenna by adding a hot load to the front of the feed. Note that we have no means of measuring DC offsets in the WVR detection system, so all such offsets are assumed to be zero. Our new WVR design for the EVLA will have a ‘‘dark current’’ switch to enable DC offsets to be measured (Chandler et al. 2004).

The field tests of the WVRs comprise an observation of a strong astronomical source such as 3C84 with a short integration time (between 1.7 and 10 seconds) while simultaneously saving WVR data using the VLA Monitor and Control system. Test data have been obtained during a 1-year period from February 2003

to January 2004 under various weather conditions and for different baseline lengths, at the default VLA continuum frequencies for X, U, K, and Q bands.

2.5. Data Processing

The measured astronomical phase on a baseline, ϕ , includes differential phase variations due to the source, the troposphere, and contributions from the electronics of both antennas. For normal interferometric operation with many antennas these can be calibrated by observing a source with known structure and position, and using phase closure relationships relative to a reference antenna. For these tests we have only one baseline, and our goal is to isolate the phase fluctuations due to the troposphere on that baseline. We have therefore taken out slowly-varying phase drifts due to the electronics and source structure by smoothing the raw phase data using a boxcar, and subtracting the smoothed data from the raw phases to form a high-pass boxcar filter. The same process is applied to the output from the WVRs, ΔT_{diff} , in order to eliminate the slowly-varying contributions to V_{off} (and V_{on}) from the receivers and from spillover.

The quantity $V_{\text{on}} - V_{\text{off}}$ is small compared to V_{off} , the measurement of which is dominated by thermal noise and the resolution of the digitizer, rather than $1/f$ noise. It must be averaged over some time period in order to increase the signal-to-noise ratio (SNR) prior to forming the observable. Note that Butler (1999) did not consider this time averaging, which had a significant bearing on his conclusions about whether water vapour radiometry would work for the VLA. We then either assume values for the weights, w , as described in § 1, and use the correlation between ϕ and ΔT_{diff} to derive a scaling factor, A (deg/K), over some timescale, or fit for all six values of w (three per antenna). While this latter is likely to give the best correlation between the WVR differential output and ϕ , we lose information about the absolute value of A , which is useful for comparisons with the predictions from atmospheric models.

The various steps of the processing applied to the test data can be summarized as follows:

1. smooth $V_{\text{on}} - V_{\text{off}}$ to increase the SNR for calibration
2. scale channel outputs by the appropriate $T_{\text{cal}}/\langle V_{\text{on}} - V_{\text{off}} \rangle$
3. either use fixed weights:
 - fix the weights to be $w_1 = -0.5$, $w_2 = 1.0$, and $w_3 = -0.5$
 - form observables and ΔT_{diff} for each time stamp
 - pass ΔT_{diff} and ϕ through a high-pass filter
 - smooth ΔT_{diff} to increase SNR
 - fit for the scaling factor, A , on a particular timescale

or fit for the weights:

- pass individual channel data, $T_{1,2,3}$, and ϕ through a high-pass filter
- smooth $T_{1,2,3}$ to increase SNR
- fit for the weights, w , on a particular timescale

3. RESULTS

3.1. Instrument Stability

Various stability measurements were made in the laboratory, initially using a temperature-regulated noise diode as a stable source, and eventually using a K-band receiver with a hot load attached to the front of its feed. In both cases, the noise source was switched into the signal path as described in § 2.3. The stability of the signal path on different timescales, τ , was characterized by the Allan Standard Deviation (ASD), $\sigma_V(\tau)$, defined by

$$\sigma_V^2(\tau) = \langle (V(t) - V(t - \tau))^2 \rangle.$$

Plots of both single channel ASDs and channel difference ASDs are presented for tests using a K-band receiver in the top two panels of Figure 3. In these plots the ASDs are normalized with respect to the mean values, $\langle V(t) \rangle$ or $\langle V_1(t) + V_2(t) \rangle / 2$ for the single and difference measurements respectively. The middle panels show actual channel data (left), difference data (center) and the righthand panel shows the variation of the ambient temperature, the temperature of the hot load, and the temperature of temperature-stabilized plate vs. time. The bottom panels show channel-channel plots, channel-temperature plots and temperature ASDs.

Since the single channel ASDs also include the stability of the load, the relevant measure of the intrinsic stability of the signal path is the channel difference ASD. The measured gain stability is therefore $\Delta g/g \sim 4\text{--}8 \times 10^{-5}$ on timescales $t \lesssim 10^3$ seconds, exceeding the required gain stability by almost an order of magnitude.

3.2. Single Baseline Field Tests

There are optimal smoothing times for the various procedures described in § 2.5. For a typical value $T_{\text{cal}} \sim 0.04T_{\text{sys}}$, $\langle V_{\text{on}} - V_{\text{off}} \rangle$ needs to be smoothed over $\sim (1/0.04)^2$ integrations (~ 520 sec) in order for the SNR to be comparable to that of a single WVR integration. Empirically we find that a value $t_{\text{smooth}} \gtrsim 10$ min is needed in order for the calibration not to significantly degrade the signal-to-noise ratio of the WVR output, consistent with this estimate. For smoothing ΔT_{diff} or $T_{1,2,3}$ in order to increase the SNR without removing high frequency structure in the water vapour fluctuations, $t_{\text{smooth}} \sim 20$ sec. When fitting for the correlation between ϕ and ΔT_{diff} similar results were obtained for fitting timescales from ~ 5 min to 1 hour, and the timescale used for the boxcar high-pass filter gave a lower rms in the corrected phase data for shorter filter times. The results presented here use $t_{\text{fitting}} = t_{\text{filter}} = 10$ min, in order to simulate a typical high frequency VLA observation with calibration observations every 10 minutes or so.

We find that applying a correction derived from the WVR outputs always improves the rms phase of the VLA data, and that this is the case at all four frequencies tested. The best correlation between ϕ and ΔT_{diff} occurs for clear skies. The correlation between ϕ and ΔT_{diff} is poor when the tropospheric phase stability is very good, for which the fluctuations in ϕ are instead limited by the stability of the VLA electronics. The correlation between ϕ and ΔT_{diff} is highly variable on days with cloud, indicating that a 3-channel WVR with closely-spaced channels can be contaminated by the emission from liquid water. Figures 4–6 show three examples of the WVR results for different baseline lengths, weather conditions, and observing frequencies.

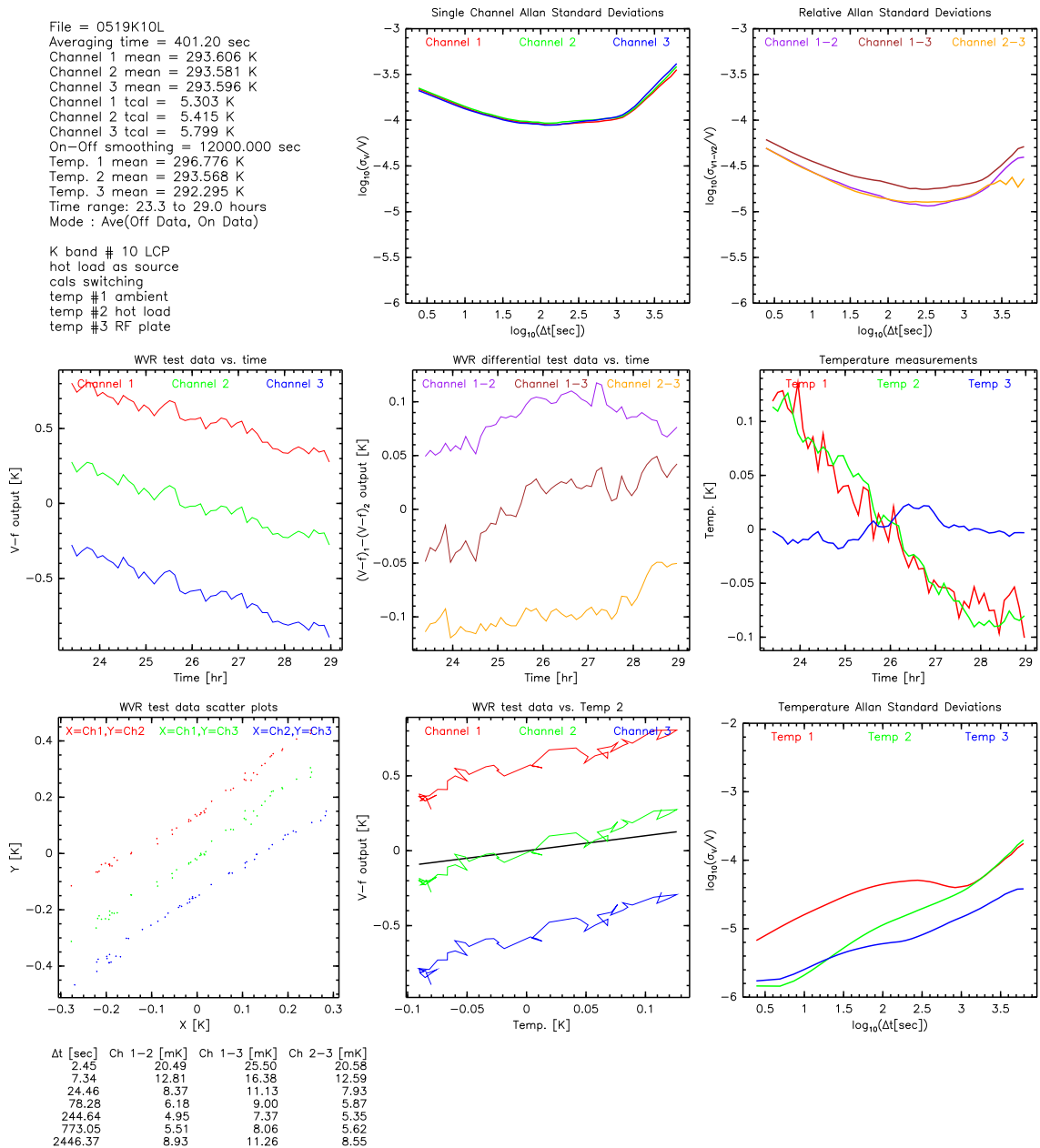


Figure 3: Laboratory test results for a WVR using a K-band receiver with a hot load attached to the front of its feed as a source. The plots shown here characterize the stability of the WVR. See § 3.1 for descriptions of the individual panels. For the panels in the middle row, and the bottom left and center panels, the mean values have been subtracted for display purposes. Channels #1 and #3 have also been displaced for display purposes. The channel mean values are printed in the text at the top left. The center panel, bottom row, also shows in black the expected slope for the channel output being equal to the temperature of the hot load.

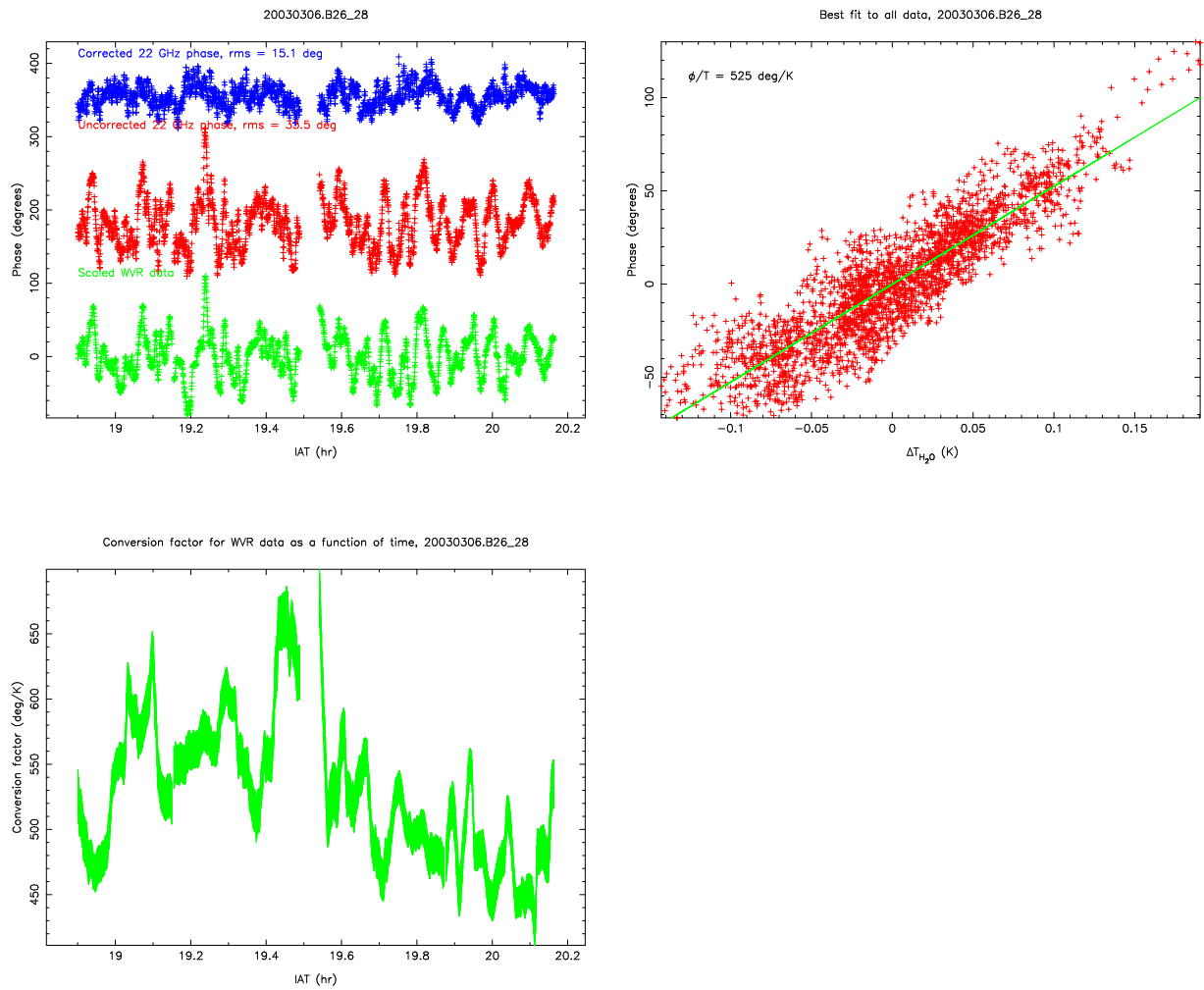


Figure 4: *Upper left:* Uncorrected phase (red, middle), scaled WVR output (green, bottom), and the phase after being corrected using the scaled WVR output (blue, top) for a baseline length of 800 m, clear skies, and an observing frequency of 22 GHz. *Upper right:* Plot of the WVR output vs. uncorrected astronomical phase for the whole time period shown. *Lower left:* Values of the scaling factor, A , calculated using a 10-min running mean, as a function of time. Note that both the phase data and the WVR output have been passed through a 10-min high-pass, boxcar filter, before deriving A .

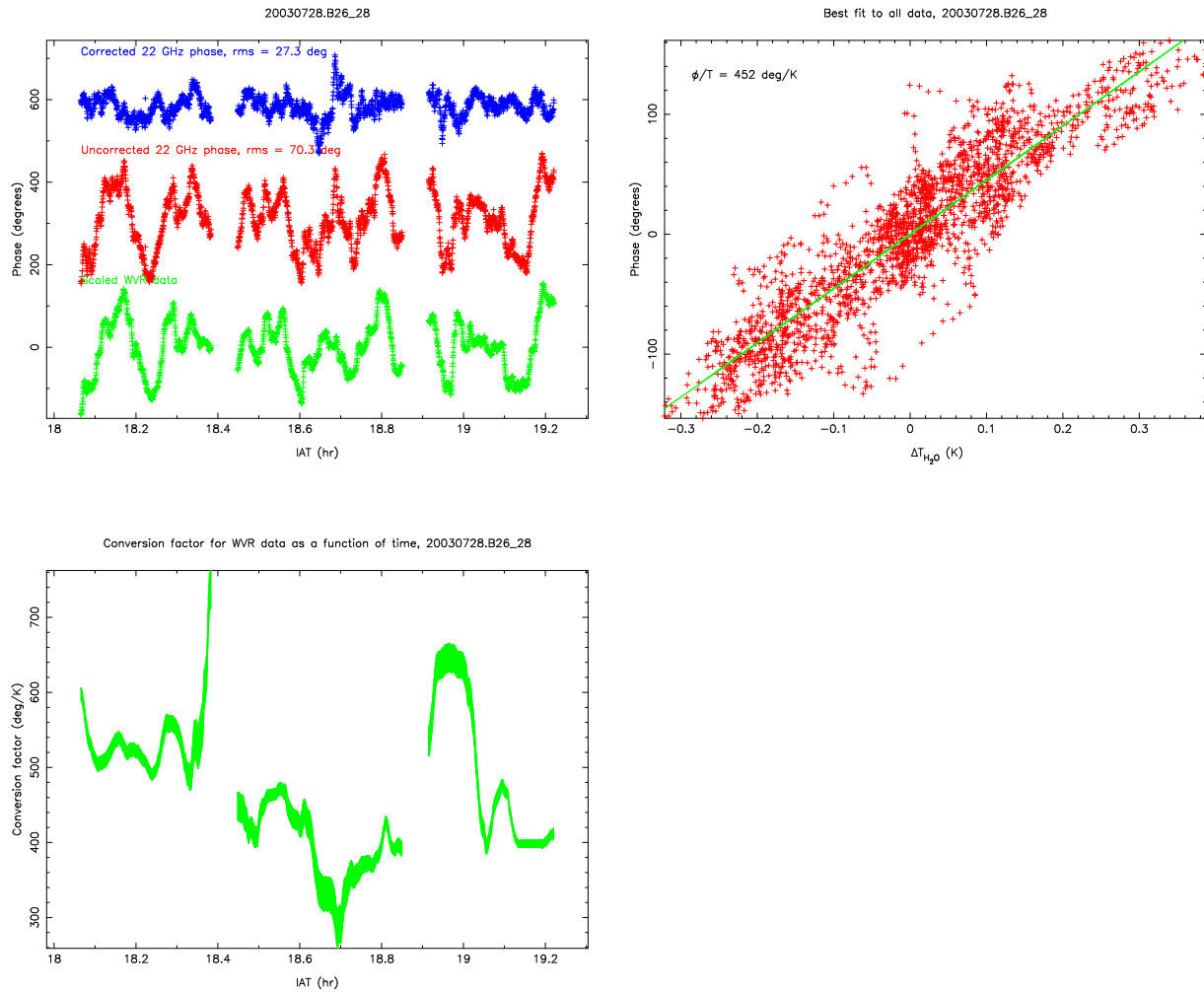


Figure 5: Same as Figure 4, but for a baseline length of 2.5 km, sky cover 50–75% with forming cumulus, and an observing frequency of 22 GHz.

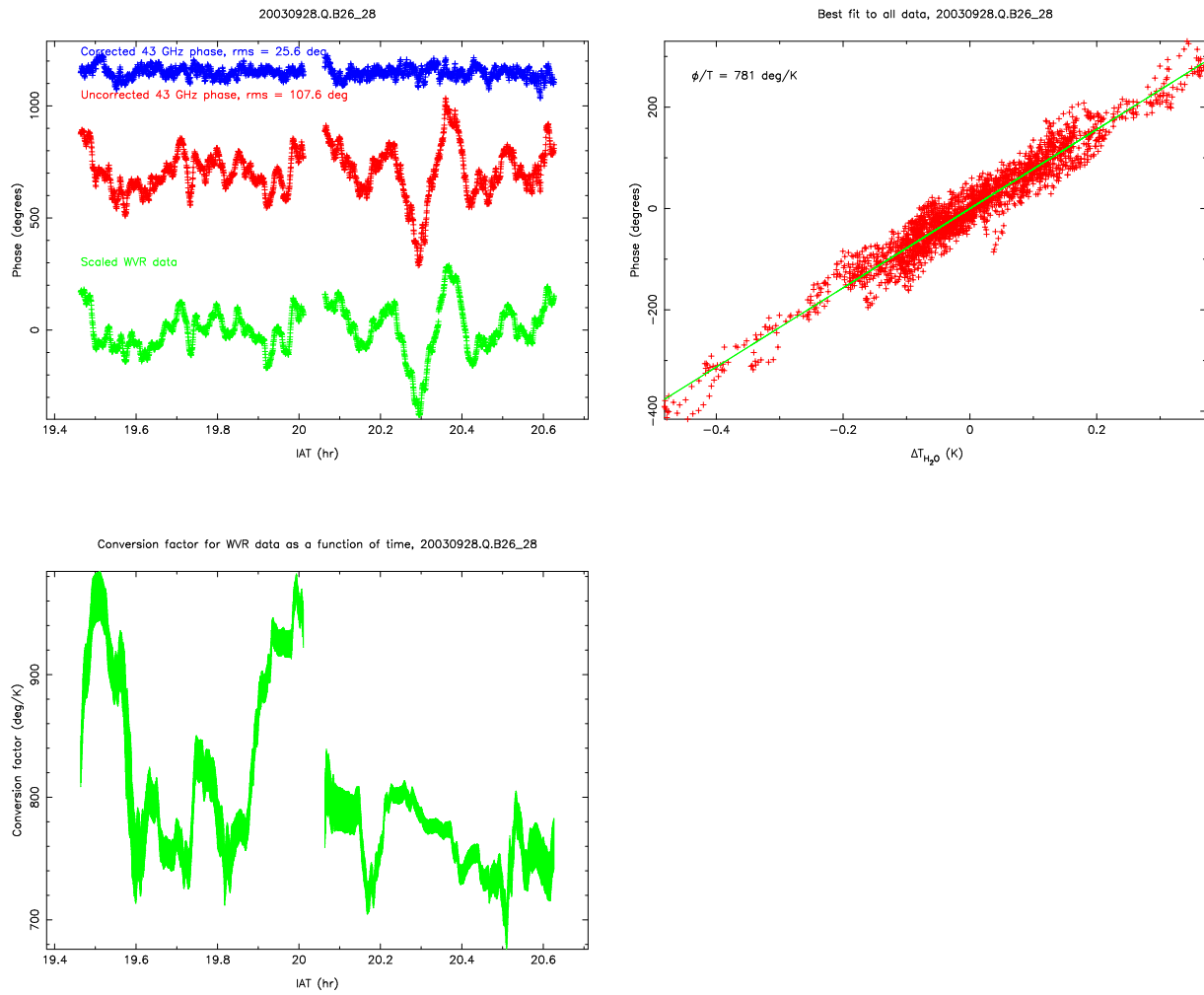


Figure 6: Same as Figure 4, but for a baseline length of 6 km, sky clear, and an observing frequency of 43 GHz.

While we find excellent correlations between ϕ and ΔT_{diff} for clear skies, the values of A obtained from these measurements are typically a factor of 1.5–2 higher than are predicted by the atmospheric models considered by Butler (1999). For example, for the channel placement given in Figure 1 the models predict $A \sim 230$ deg/K at 22 GHz, while $A \sim 400$ deg/K is actually observed. Interestingly, experiments at the Owens Valley Millimeter Array using a three-channel 22 GHz WVR system show a similar discrepancy from the expected value (D. Woody, personal communication). Figure 7 shows the distribution of A for all the good observations obtained during the year of tests, for which the rms phase was large enough to be clearly dominated by the troposphere rather than the VLA electronics. The data have been separated into “clear” and “cloudy” datasets, based on the weather information entered into the operator log for each observation. Here, clear weather also includes observations for which the sky cover is given in the logs as $\leq 10\%$ stratus cloud. While these classifications are somewhat objective and may be operator dependent, they are the best measure we have of the potential contributions from liquid water.

The most data have been obtained for an observing frequency of 22 GHz. Here the distribution of A is clearly singly peaked for the clear data, but seems to be bimodal for the cloudy data, with peaks around $A \sim 400$ and ~ 0 deg/K (i.e., no correlation between ϕ and ΔT_{diff}). At $\nu = 43$ GHz the clear data are again singly peaked, with the median value of A scaling linearly with frequency compared with $\nu = 22$ GHz, as expected for the non-dispersive troposphere. The 43 GHz cloudy data, on the other hand, exhibit a very broad distribution. No clear data are available for $\nu = 15$ GHz, but extrapolating from the median values obtained at the other three frequencies we would expect $A \sim 270$ deg/K. Only clear data are available at $\nu = 8$ GHz, for which the distribution in A is singly peaked, with a median value in line with scaling linearly with frequency from both the 22 and 43 GHz values.

The fact that the median values of A for the clear datasets scale so well with frequency supports the idea that the phase fluctuations originate in a non-dispersive medium. However, the fact that the values of A are $\sim 70\%$ higher than predicted by atmospheric models for water vapour alone suggests there may be another contribution to the excess path experienced by the incoming radio waves, correlated with the water vapour. The most likely candidate is the dry atmosphere (A. Stirling, personal communication), which contributes electrical path length L_{dry} (cm) $\simeq 0.228P_0$ where P_0 is the surface pressure in millibars (Thompson, Moran, & Swenson 2001). Thus a typical value $P_0 \sim 10^3$ mbar contributes a total of 230 cm of electrical path. A fluctuation in L_{dry} of one part in 10^3 is therefore equivalent to 1 radian of phase at $\nu = 22$ GHz. Fluctuations in temperature (and therefore pressure) are responsible for seeing at optical and infrared wavelengths, although the turbulence responsible for these fluctuations is typically confined to relatively narrow layers in the troposphere (e.g., Coulman 1985). Such turbulence in the dry component, however, will also bring along with it fluctuations in the associated water vapour, and it is interesting to note that the value of Fried’s parameter, r_0 , derived from 22 GHz phase stability measurements is in reasonably good agreement with that expected by extrapolating from optical and infrared measurements (Cornwell 1984).

Further work is needed in order to establish whether there is a correlation between optical seeing and ϕ or ΔT_{diff} at the VLA site, and to assess the importance of the dry atmosphere as a source of phase fluctuations at millimeter wavelengths. From a pragmatic viewpoint, however, as long as we are using an empirically-derived value for A that improves the phase RMS, understanding the origin of the phase fluctuations is less important. The success of the WVR tests to date has led to a revised design for the WVRs to be implemented for the EVLA, and is described by Chandler et al. (2004).

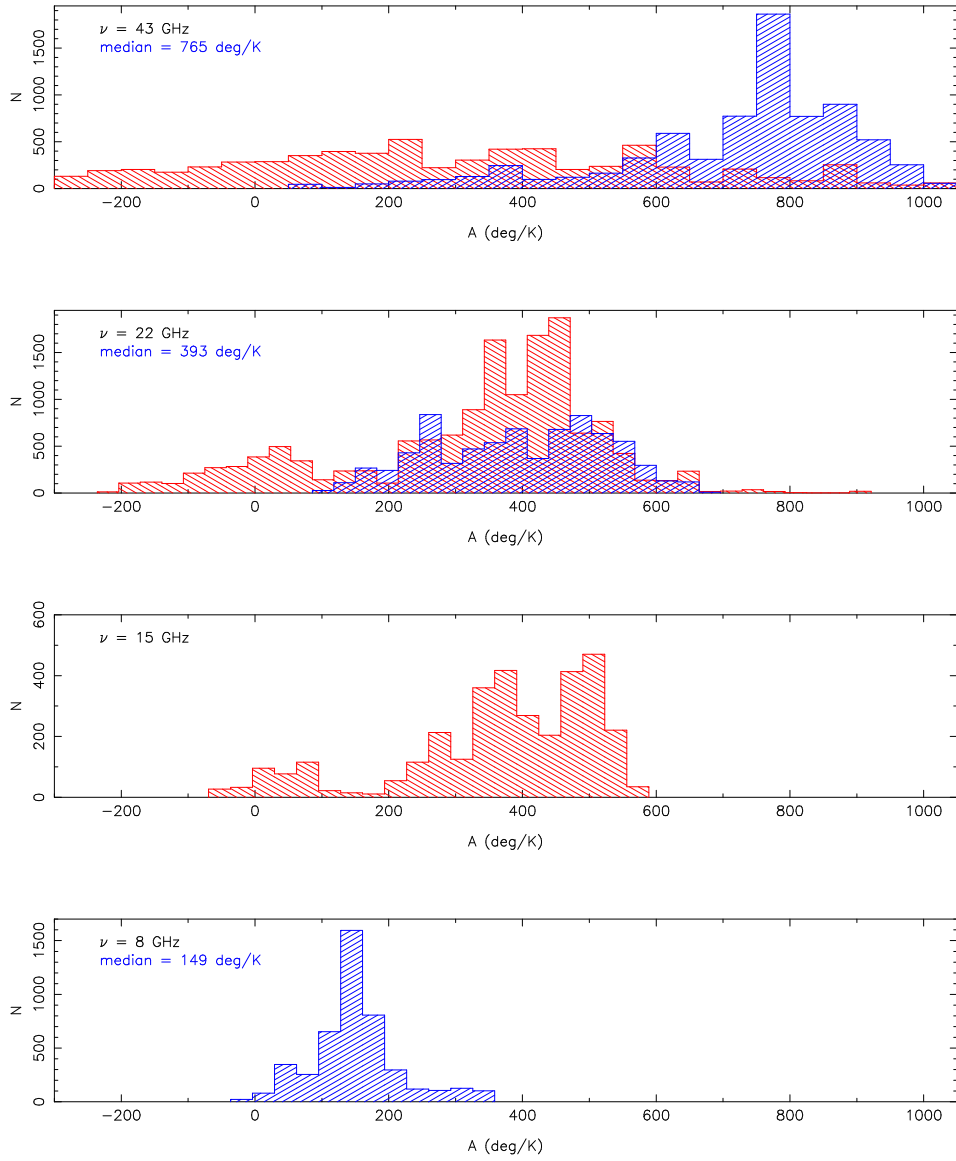


Figure 7: Histograms of A at the four different observing frequencies, derived on 10-min timescales for clear (blue) and cloudy (red) skies.

REFERENCES

- Butler, B. 1999, VLA Scientific Memo # 177
- Chandler, C. J., Brisken, W. F., Butler, B. J., Hayward, R. H., Morgan, M., & Willoughby, B. E. 2004, EVLA Memo # 74
- Cornwell, T. J. 1984, ALMA Memo # 13
- Coulman, C. E. 1985, ARA&A, 23, 19
- Thompson, A. R., Moran, J. M., & Swenson, G. W. 2001, Interferometry and Synthesis in Radio Astronomy, 2nd Edition (New York: John Wiley & Sons, Inc.), 513